Numerical study and semi-analytical model of rocket motor exhaust backflow in rarefied atmosphere

Antoine Clout,[1, a)] Adrien Langenais,[1] Yann Dauvois,[2] Luc Mieussens,[3] and Julien Labaune[1]
[1)] *DMPE, ONERA, Université Paris Saclay 91120 Palaiseau, France*
[2)] *DMPE, ONERA, Université de Toulouse, 31000 Toulouse - France*
[3)] *Bordeaux INP, Univ. Bordeaux, CNRS, IMB, UMR 5251, F-33400 Talence, France*

(Dated: 22 November 2024)

The prediction of backflow from multi-species high density rocket engine plume at high altitude, *i.e.* plume gases going upstream of the vehicle in rarefied atmospheric conditions remains a challenging numerical problem. Direct Simulation Monte Carlo computations are used to assess the sensitivity of backflow to plume and atmosphere inflow properties, and ultimately to derive a semi-analytical backflow model. It is found that backflow is independent of plume density in the thermal equilibrium limit at the nozzle exit plane, which allows for huge computational cost reductions in simulations to determine the backflow model parameters. The backflow behaviour also appears to be dependent on two Knudsen numbers, representing the density effect in the far field atmosphere and in the compressed region in front of the vehicle. The ability of the model to estimate the backflow of specific species is finally demonstrated on a meter sized solid rocket case.

I. INTRODUCTION

Simulation of high temperature and high density rocket plume flow at high altitude is performed for several purposes. For military applications, the signature of missile in the infrared spectrum[1] or in the radar spectrum[2] is of great importance. This radar signature originates from the ionisation of the gases in the plume, which can also induce absorption of the communication signals between the ground stations and the launcher[3]. This last phenomenon, called blackout, is studied for both civil and military applications. Finally, another phenomenon of great interest is backflow, which corresponds to plume gases going upstream of the vehicle. Thruster exhausts can indeed expand to large angles and become a primary source of contamination for satellite surfaces, including solar panels, leading to a reduction of their power output. This backflow therefore manifests itself by a particle and heat flux on the walls of the vehicle. If the vehicle has its fearing off, it means the payload is directly exposed to some of the plume gases and can easily be contaminated.

Rocket plumes have been studied using classical Computational Fluid Dynamics (CFD) methods based on a resolution of the Navier-Stokes equations through a finite volume approach. This resolution is usually made through a Reynolds-Averaged Navier-Stokes (RANS)[4,5] or Large-Eddy Simulation (LES)[6,7] approach. The Navier-Stokes equations nonetheless have an underlying continuity hypothesis of the medium, therefore as the altitude of the rocket increases, *i.e.* as the atmosphere rarefies, these equations start deviating from their domain of validity. Some physical phenomena, such as backflow, are consequently not properly represented. This backflow was first studied experimentally[8–11], and semi-analytical models were then developed. The first model, by Boraas[12] in 1987, assumes that the fluid is continuous at the Nozzle Exit Plan and in a cone called continuous cone, which is considered to be the source of all backflow. Using these assumptions and some geometrical considerations, the mass flux of plume gases going upstream of the vehicle can be estimated. Due to the computational limitations of the 1980's and the difficulty of realising backflow experiments, this model has not been validated. A second model for backflow estimation has been developed in 1994 by Jenkins, Ciucci, and Cochran[13]. Contrary to the first one, it assumes the flow is continuous downstream of the vehicle only in a region defined by the mean free path of the particles, which is more physical. However as for the first model it assumes the flow in the rarefied region to be collisionless, and is only applicable to single species flows. Finally, neither model take into account atmospheric effects. Jenkins *et al.* [13] conclude that the best way to predict backflow is to solve the Boltzmann Transport Equation (BTE) with Direct Simulation Monte Carlo (DSMC)[14].

The BTE is valid at any degrees of rarefactions, which is suitable for plume flows and therefore backflow problems, but its resolution through the statistical approach of Direct Simulation Monte Carlo (DSMC)[14] is extremely costly in dense regions such as plume cores. Some DSMC simulations of small thrusters backflow were still performed[15–17]. These studies focused on low density low temperature thrusters, mainly used for attitude control, and larger scale DSMC simulations focusing on backflow from dense plume flows are still lacking in the literature. For that purpose, hybrid methods are used, where the dense core of the plume is treated with the Navier-Stokes equations and the rarefied atmosphere and expansion region are treated with the BTE through a DSMC approach. This method has been developed by Schwartzentruber and Boyd[18] for hypersonic flows and is widely used for rocket plumes applications[19–26].

[a)] Electronic mail: antoine.clout@onera.fr

In a previous work[27], a one-way coupled Navier-Stokes to DSMC simulation of JAXA's M-V third stage[28] has been carried out. It has been found that the DSMC solution, contrary to the standalone Navier-Stokes solution, gives a strong backflow of light species towards the front of the vehicle. This can be observed in Figure 1, where X_l, the mole fraction of H_2 which is the lightest species in the simulation, is represented for the DSMC solution. The black hatched region of the domain in the bottom right hand corner corresponds to the continuous region and is not treated by the DSMC solver. The interface with the rarefied region is used as an input to the DSMC computation. This result was obtained by performing the exact methodology described in reference 27 with revised collision properties in the DSMC simulation, longer statistical averaging, larger number of particles and finer mesh. This simulation reproduces atmospheric conditions at an altitude of 183 km, altitude at which the rocket fearing protecting the payload is usually off. This indicates that backflow is not limited to small thrusters used for attitude control in vacuum, but is also occurring for light species of larger solid rocket engines at high altitude. This is in agreement with Hueser's *et al.* work[15]. Moreover, differences in behaviour between light and heavy species in rarefied dynamics is a known subject, for instance Sabouri[29] showed that light and heavy species segregate in rarefied divergent micro-nozzles.

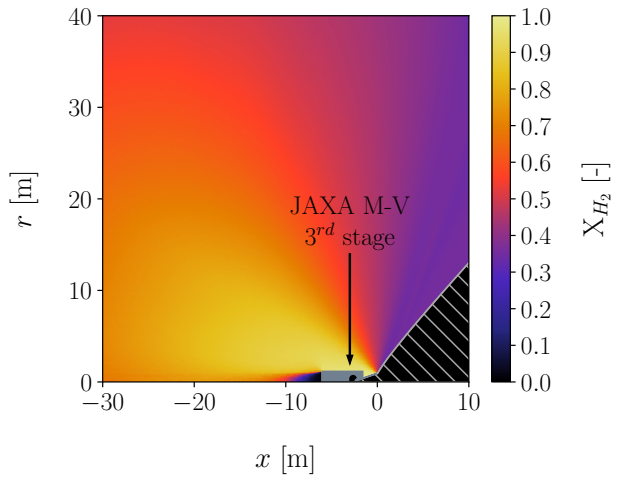

FIG. 1: Molar fraction of H_2 around the third stage of JAXA's M-V rocket computed using the DSMC method. The black hatched region is treated with a Navier-Stokes solver.

This paper aims at better understanding backflow of high density, temperature and exit velocity plumes generated by this kind of thrusters. First the main aspects of the DSMC method are presented in Section II A, followed by the numerical setup used through the whole paper in Section II B. A reference DSMC simulation is conducted and analysed in Section III. In Section IV a semi analytical model to predict backflow is developed: in Section IV A a non-dimensional parameter is derived, in Section IV B the sensitivity of the backflow problem to this parameter is assessed, in Section IV C a model for single species plume is presented, in Section IV D the model is extended to multi-species plumes, in Section IV E backflow sensitivity to plume density is determined, in Section IV F the impact of atmospheric density on backflow is evaluated, and the general methodology for backflow estimation is presented in Section IV G. An application of the model to the JAXA's M-V third stage is finally attempted in Section V. Concluding remarks are finally presented in Section VI.

II. SIMULATION METHODOLOGY

A. Direct Simulation Monte Carlo

The DSMC method, thoroughly described by Bird in[14], is based on simulating numerical particles, each representing a large ensemble of physical particles. The motion of the numerical particles is decoupled from their collisions in each timestep. This implies the two following required conditions:

1. Every grid cell shall be smaller than the particles' mean free path λ.

2. The simulation timestep shall be smaller than the mean collision time.

Macroscopic quantities are obtained by averaging particle properties in each cell for a large number of timesteps. To ensure statistical representativity, a third numerical condition is needed.

3. Every grid cell shall contain at least 10 numerical particles of each species.

In the present work, DSMC simulations are conducted over a two dimensional, axisymmetric domain, using the open source code SPARTA[30] developed by Sandia National Laboratories. To ensure criterion 1 is respected, SPARTA's Adaptive Mesh Refinement (AMR) capability is used. Since the mesh is represented as a quadtree, each cell can be subdivided independently.

Moreover, due to the large rarefaction and nonequilibrium effects in high altitude plume flows the Variable Soft Sphere[31] (VSS) collision model, as well as the internal energy exchange Borgnakke and Larsen[32] model are used. The VSS collision model allows for uncoupled viscosity and diffusivity dependency on temperature, which is needed on cases with wide temperature range. Chemical reactions are not considered due to the large rarefaction effects at high altitude, to the small temperature of plume flows after expansion in the divergent, and to the relatively small velocities of ascending space vehicles compared to re-entry vehicles.

Rotational relaxation, as detailed in Bird's book[14], is proportional to a rotational collision number Z_{rot} according to Parker's law[33]:

$$Z_{\text{rot}} = \frac{Z_{\text{rot}}^{\infty}}{1 + \frac{\sqrt{\pi}}{2}\sqrt{\frac{T^*}{T_{\text{tr}}}} + \left(\pi + \frac{\pi^2}{4}\right)\frac{T^*}{T_{\text{tr}}}} \tag{1}$$

This number represent the mean number of collision a particle must endure to transfer rotational energy to translation energy modes. It increases with the translational temperature of said particle.

Similarly, vibrational relaxation is proportional to a vibrational collision number Z_{vib} as by Millikan and White[34], and decreases with translational temperature:

$$Z_{\text{vib}} = \frac{C_1}{T^{\omega}} \cdot \exp\left(C_2 \cdot T^{-1/3}\right) \tag{2}$$

B. Computational setup

Due to the large scale and high density of the JAXA's M-V third stage presented in Section I, full DSMC simulations on this case are unaffordable. A simpler vehicle called *reference case* or *REF* in legends is therefore introduced to reduce computational cost. It consists of a reduced geometry of a rocket stage with a diameter equal to one tenth of the one from JAXA's M-V third stage[35], *i.e.* $R = 0.0931\,\text{m}$ as depicted in Figure 2.

The combustion chamber as well as the convergent-divergent nozzle are not simulated and plume gas are injected at the Nozzle Exit Plane (NEP) of the engine. This boundary is discretized into 10 equal length (9.31 mm) segments as depicted in Figure 3. The inflow conditions on each segment are taken from a RANS solution computed in the previous work in reference 27. The plume density is reduced by a factor of 100 therefore the mean plume Knudsen number $\text{Kn}_{\text{plume}} = \lambda_{\text{plume}}/R = 8.1 \times 10^{-2}$ to decrease computational cost. The corresponding velocities, temperatures and number densities are reported in Table I.

It operates in the same atmospheric conditions as JAXA's case, *i.e.* the altitude of simulation is 183 km which according to the US AirForce Standard Atmosphere[36] corresponds to a static temperature $T = 800\,\text{K}$. The number density is $n = 1.255 \times 10^{16}\,\text{m}^{-3}$, corresponding to an atmospheric Knudsen number $\text{Kn}_{\text{atmo}} = \lambda_{\text{atmo}}/R \approx 10^3$. The velocity of the vehicle is $(u, v) = (6100, 0)\,\text{m s}^{-1}$, which corresponds[28] to a Mach number of 10.6. The simulation domain extends in the range $(x, r) \in [-15, 10] \times [0, 15]\ \text{m}^2$, with the bottom of the NEP at $(x, r) = (0, 0)$. The walls of the vehicle are at a constant temperature of 500 K with an accommodation coefficient of 1.

To decrease computational time, the atmosphere is only modelled with N_2, injected over the left and top boundaries of the domain as depicted with the blue arrows in Figure 2. The plume is represented using H_2 as a light species and N_2 as a heavy species, because its molecular mass is extremely close to the molecular mass of the plume mix of JAXA's rocket when H_2 is removed. All particles' and collisions' DSMC parameters used by SPARTA are summarized in Table II. The composition of the plume is constant for all segments, with a molar fraction of light species of 0.34. The two vibrational parameters of the light species are chosen so that relaxation is 4 times faster than the heavy species', as shown

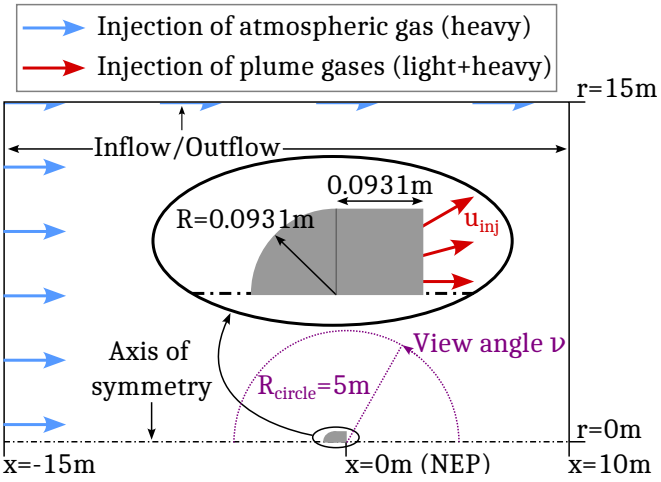

FIG. 2: Schematic view of the reference case geometry and boundary conditions. All dimensions are in meters. The ellipse corresponds to a zoomed-in view.

FIG. 3: Representation of the inflow segments along the NEP.

TABLE I: Plume inflow properties. The segments correspond to the ones depicted in Figure 3.

Segment ID	u_{inj} [m s^{-1}]	v_{inj} [m s^{-1}]	T [K]	$n \cdot 10^{-21}$ [m^{-3}]
0	2791	0	1417	1.815
1	2757	152	1417	1.820
2	2743	242	1396	1.860
3	2748	333	1357	1.939
4	2801	430	1298	2.055
5	2863	534	1231	2.180
6	2915	641	1169	2.301
7	2979	744	1107	2.474
8	3072	865	1019	2.718
9	2970	928	1250	2.494

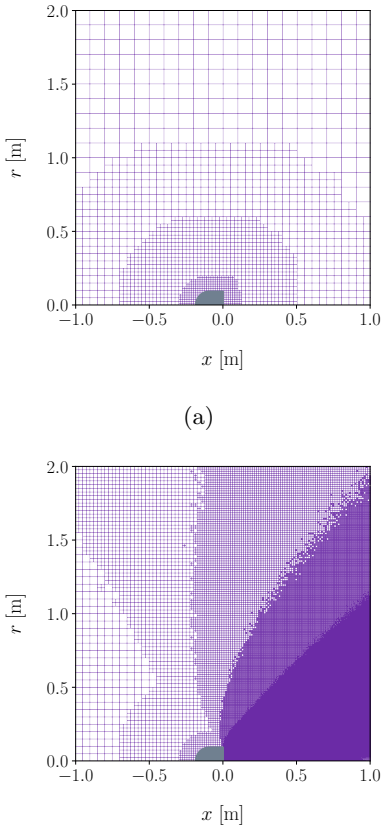

FIG. 4: Zoomed-in view on (a) the initial mesh before AMR and (b) the final mesh after AMR used for the simulation.

by Chatelet *et al.* [37]. The number of degrees of freedom in rotation and vibration is set to 2 due to the geometry of diatomic molecules.

The initial mesh is composed of square cells of 10 cm sides, with refinement close to the vehicle, as illustrated in Figure 4a. The AMR method splits a cell in 4 equal size sub-cells if the local Knudsen number $\mathrm{Kn}_{\mathrm{loc}} = \lambda_{\mathrm{loc}}/dx_{\mathrm{cell}}$, *i.e.* the ratio of the local mean free path by the cell side length, is larger than 2, which ensure Criterion 1. The resulting mesh close to the vehicle is shown in Figure 4b.

The simulation timestep is set to 5×10^{-8} s to respect Criterion 2 since the mean collision time at NEP is around 1×10^{-7} s. The numerical representativity parameter is set to 1×10^{13} to ensure Criterion 3, *i.e.* at least 10 particles of each species are present in each cell. The total number of particles in the simulation is around 147 millions. The averaging of cell properties is performed over 400 000 iterations, *i.e.* 0.02 s. This duration corresponds to around 60 m of mean travel of plume gas, and 120 m of atmospheric gas, which is more than the domain size.

III. MAIN FLOW FEATURES

Figure 5 shows the molar fraction field of both heavy and light plume species around the vehicle. It can be noted that both species do not expand in the same way. The heavy specie expands in a cone and does not flow upstream of the vehicle as shown in Figure 5a. On the other hand the plume light species, in a similar manner as Figure 1, flows upstream which corresponds in Figure 5b to a non zero value of X_l on the side of the vehicle. It can also be noted that the vehicle's walls block some of the plume particles which explains the black region just in front of the vehicle in Figure 5c.

In the following, backflow is defined as all species emitted from the plume that go upstream, *i.e.* that provide a mass flux ϕ_m [$\mathrm{kg\,m^{-2}\,s^{-1}}$] at view angles larger than 90° across the dotted semi-circle of Figure 2. Several radii have been investigated, without any meaningful difference between each one, therefore $R_{\mathrm{circle}} = 5$ m is chosen since it corresponds to half the distance between NEP and the right hand side of the domain. Is has been checked that the integral over the 180° that ν can reach is equal to the total injected mass flux at NEP. The difference in backflow of light and heavy species can be quantitatively observed in Figure 6, where the normalized outwards mass flux of plume species Φ_m, *i.e.* the outwards mass flux divided by the total mass flux, is plotted for all view angles ν. From this, one can compute for each species independently the total backflowing normalized mass flux, denoted Backflow number Ba in the following:

$$\mathrm{Ba} = \frac{\dot{m}_{\mathrm{backflow}}}{\dot{m}_{\mathrm{tot}}} = \frac{\int_{90}^{180} \phi_m(\nu) d\nu}{\int_{0}^{180} \phi_m(\nu) d\nu} = \int_{90}^{180} \Phi_m(\nu) d\nu \quad (3)$$

A low value of Ba corresponds to no or few backflow, while a large value corresponds to important backflow. A value of $\mathrm{Ba}_h = 4 \times 10^{-8}$ is found from the DSMC simulation, which indicates that the heavy species does not backflow. On the other hand the backflow number for light species is $\mathrm{Ba}_l = 2.6 \times 10^{-2}$.

Since the injection at NEP originates from a CFD simulation which assumes thermal equilibrium, the particles are injected according to a Maxwellian distribution centred on the injection velocity u_{inj} and with a standard deviation of $\sqrt{k_{\mathrm{B}}T/m}$, where k_{B} is the Boltzmann constant, T the translational temperature of the gas and m the mass of the species. Therefore the standard deviation of the velocity distribution function is only influenced by the temperature of the fluid and the mass of the particles. Since both types of particles are injected with the same temperature, only the difference in mass can explain this difference in backflowing properties. The light species therefore has a broader velocity distribution, which means more particles with negative x-velocity (denoted u), which could backflow. This can be seen in Figure 7, which shows the Probability Den-

TABLE II: Species DSMC parameters.

Parameter	Unit	Light species	Heavy species	Reference
Reference molecule		H_2	N_2	
Molecular mass	[kg]	3.3471×10^{-27}	4.6518×10^{-26}	
Reference collision diameter d_{ref}	[m]	2.88×10^{-10}	4.11×10^{-10}	14
VSS temperature viscosity index ω_{VSS}	[-]	0.67	0.74	14
VSS scattering angle parameter α_{VSS}	[-]	1.35	1.36	14
Reference temperature T_{ref}	[m]	273	273	14
Rotational degrees of freedom	[-]	2	2	
Parker's law parameter Z_{rot}^{∞}	[-]	20	23	38 & 39
Parker's law parameter T^*	[K]	100	91.5	38 & 39
Vibrational degrees of freedom	[-]	2	2	
Vibrational temperature	[K]	6159	3371	14
Vibrational relaxation parameter C_1	[K]	9.1	9.1	14
Vibrational relaxation parameter C_2	[$K^{1/3}$]	180	220	14

sity Function (PDF) of u in the $(x, r) \in [0, 0.02] \times [0, R]$ region.

First of all, it can be observed that both PDF approximate extremely well Maxwellian distributions. This is a confirmation of the fact that the vicinity of the NEP is at local thermal equilibrium, which is consistent with the Knudsen number of the plume being lower than 10^{-2}. Then, the heavy species u distribution is almost exclusively in the positive range, with only 4×10^{-5} % of the distribution in the negative range whereas the light species distribution is composed of 8.3 % negative velocities. The mass of plume species and their temperature therefore seem to be critical regarding backflow.

The plume injection properties are dependant on the position along the NEP as stated in Table I. It is therefore critical to know where backflowing gas comes from. Figure 8 shows the outwards mass flux of plume gas with respect to the region of emission. It shows that when $\nu > 90°$, the only two regions that provide a significant amount of backflow are the two top ones, *i.e.* segments 8 and 9. When $\nu > 135°$, only the very top segment provide a significant amount of backflow. This is in agreement with Charton *et al.*[24], which showed the close lip area provides particles for the high look angle region.

Several elements can explain why backflow originates from the outer injection segments. First, if particles in segment 9 have a negative x-velocity u and a positive r-velocity v, then they will rapidly leave the core of the plume, enter a region with fewer collisions, and if not influenced by the atmosphere they will backflow. On the other hand particles originating from inner segments are in a dense region, where collisions occur regularly therefore particles with negative u and positive v are likely to collide with several particles and can stay trapped in the core of the plume. Secondly, segment 9 contains the nozzle wall boundary layer which means its average velocity is slightly smaller than other segments, shifting PDF of u in this segment to the left. Moreover, this slow down induces an increase in temperature, which broadens the PDF. These two effects combined increase the proportion of particles with a negative u compared to the other segments. It was shown that the phenomenon of backflow is highly dependent on regions close to the nozzle lip.

IV. MODEL DERIVATION AND SENSITIVITY STUDY

The aim of this section is to derive a semi-analytical model to predict the backflow number Ba, which is done by performing several sensitivity studies. First, a dimensionless number proportional to the number of particles with negative x-velocities is derived. Then backflow sensitivity to this number is assessed. A model to link Ba to this number is detailed for single species and multi-species flows. Finally the effects of plume's and atmosphere's densities are discussed.

A. Dimensionless number construction

Let us first consider a simpler case with the same geometry but only one species injected at constant T, constant u and zero v along the NEP. No atmosphere is considered here. Figures 6 and 7 suggest that a quantity of interest in the backflow problem is the number of particles with a negative u close to the NEP. This proportion is, by construction, liked to the mean value of the PDF of u and its width. Let's then consider a condition for backflow number defined as the ratio of these two quantities:

$$\mathrm{C_B} = \frac{\sqrt{\dfrac{k_\mathrm{B} T_{\text{inj}}}{m_{\text{species}}}}}{u_{\text{inj}}} \tag{4}$$

with $u_{\text{inj}} > 0$ the velocity in the x direction of plume gas at NEP, T_{inj} the translational temperature of the plume, m_{species} the species molecular mass and k_B the Boltzmann constant. The greater this number is, the more

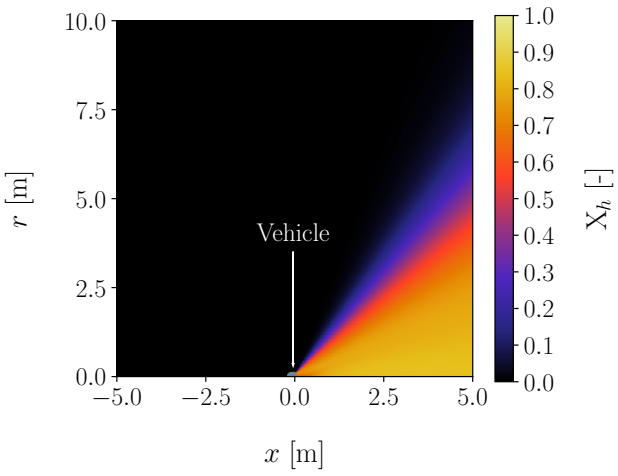

(a)

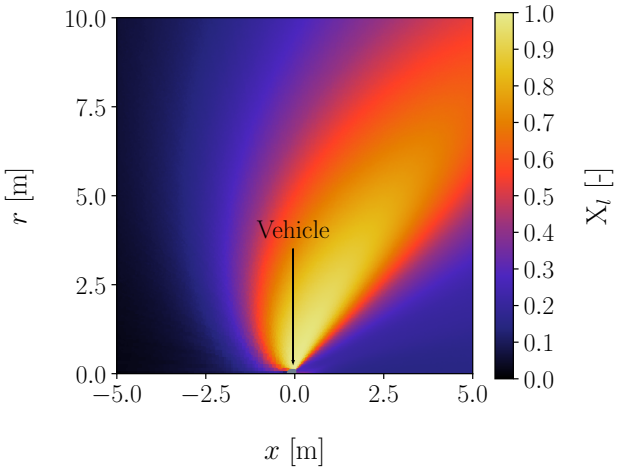

(b)

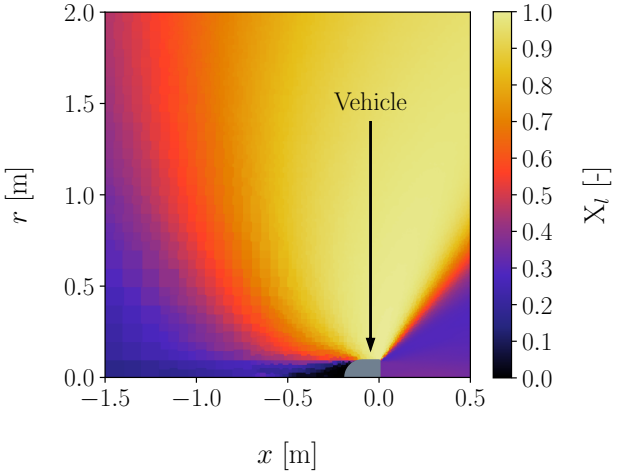

(c)

FIG. 5: Molar fraction of (a) heavy and (b, c) light species around the vehicle located in (0,0). Sub-figure (c) corresponds to a zoomed-in view.

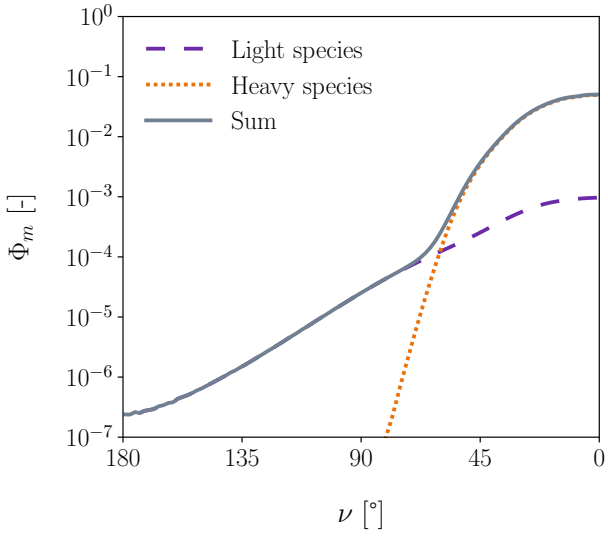

FIG. 6: Outwards normalized mass fluxes of plume gases.

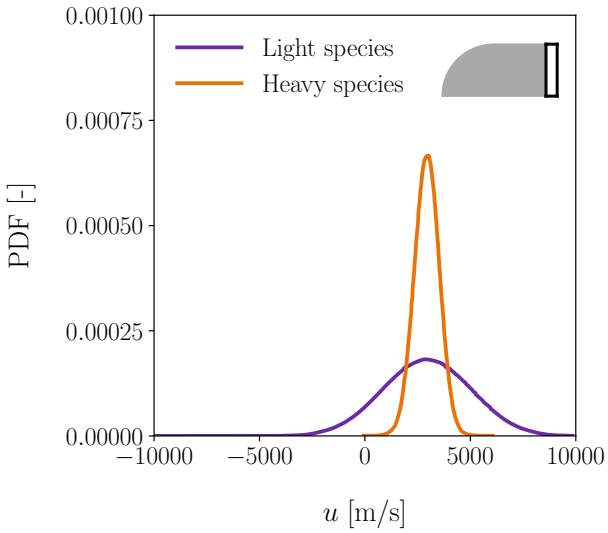

FIG. 7: Probability Density Function of particle's u-velocity in the $(x, r) \in [0, 0.02] \times [0, R]$ region depicted in the top right hand corner.

particles have a negative u. To check whether this number is an invariant of the problem, the outwards mass flux of three cases at constant C_B can be computed, with the input conditions set arbitrarily, and summarized in Table III. The rest of the properties are as in Table I.

Figure 9 represents the normalized outwards mass flux for the three cases described in Table III. Despite the completely different species mass, inlet temperature and inlet velocity, the angular mass flux, and therefore Ba, is the same for all cases. This means that C_B is a dimensionless number that seems fundamental of the backflow problem.

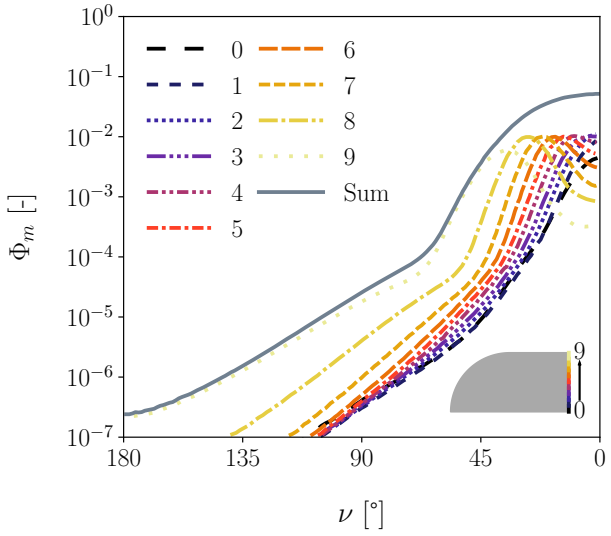

FIG. 8: Normalized outwards mass flux of plume species versus look angle at a distance of $R_{\text{circle}} = 5\,\text{m}$ depending on the emission origin, *i.e.* segments 0 to 9 as depicted in the bottom right-hand corner. The *Sum* curve corresponds to the sum of all other curves as in Figure 6.

TABLE III: Modified inflow properties.

Case	m_{species} [kg]	T_{inj} [K]	u_{inj} [m/s]	C_B
A	7.785×10^{-27}	1202	2920	0.5
B	3.347×10^{-27}	517	2920	0.5
C	3.347×10^{-27}	1202	4453	0.5

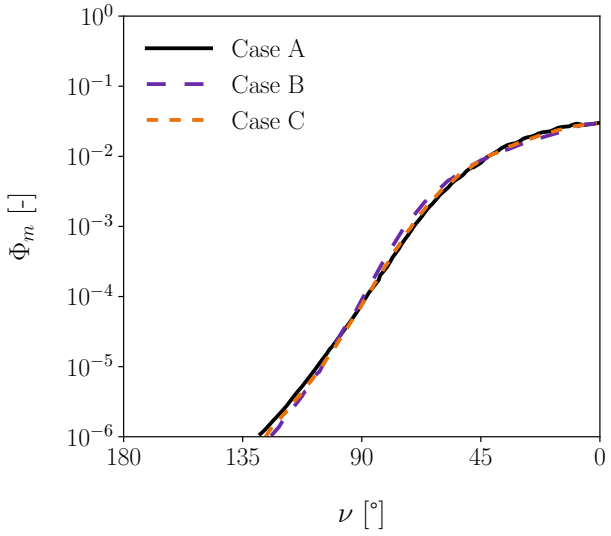

FIG. 9: Outwards normalized mass flux versus view angle for three cases with $C_B = 0.5$.

B. Backflow sensitivity on C_B

By construction, it is expected that backflow increases with C_B, since it has been observed in Section III that light species backflow more than heavy species. Figure 10 represents both the angular normalized outwards mass flux of plume gas (10a) and the backflow number (10b) for several values of C_B. The injection properties are as follows. The species mass is set to $3.347 \times 10^{-27}\,\text{kg}$, the velocity to $u = 2920\,\text{m s}^{-1}$ and the translational temperature is computed to match the corresponding C_B. As expected, backflow increases with C_B, but not linearly. At high C_B, Ba seems slightly increasing but when C_B decreases under 0.6, Ba drops rapidly. When C_B is lower than 0.4, less than 1×10^{-3} of the injected mass flux goes upstream of the vehicle, therefore backflow can be considered negligible under these conditions.

C. Model derivation for single species plume

The derivation of the model consists in estimating Ba as a function of C_B. First of all, the analytical expression of the PDF(u) in the continuum limit is:

$$PDF(u) = \frac{1}{\sqrt{2\pi\dfrac{k_B T}{m}}} \exp\left(\frac{(u-u_{\text{inj}})^2}{2\dfrac{k_B T}{m}}\right) \tag{5}$$

The fraction of particles with negative velocities follows straightfully:

$$f = \frac{\int_{-\infty}^{0} PDF(u)du}{\int_{-\infty}^{+\infty} PDF(u)du} \tag{6}$$

Using the change of variable:

$$\xi = \frac{u-u_{\text{inj}}}{\sqrt{2\dfrac{k_B T}{m}}} \tag{7}$$

f becomes:

$$\begin{aligned} f &= \frac{\int_{-\infty}^{-1/C_B\sqrt{2}} \exp(-\xi^2)d\xi}{\int_{-\infty}^{+\infty} \exp(-\xi^2)d\xi} \\ &= \frac{\int_0^{+\infty} \exp(-\xi^2)d\xi - \int_0^{1/C_B\sqrt{2}} \exp(-\xi^2)d\xi}{2\int_0^{+\infty} \exp(-\xi^2)d\xi} \\ &= \frac{1-\text{erf}\left(\dfrac{1}{C_B\sqrt{2}}\right)}{2} \\ &= \frac{\text{erf}\left(\dfrac{-1}{\sqrt{2}C_B}\right)+1}{2} \end{aligned} \tag{8}$$

Equation (8) means that the fraction of particles with negative u depends only on C_B. However, not all of these

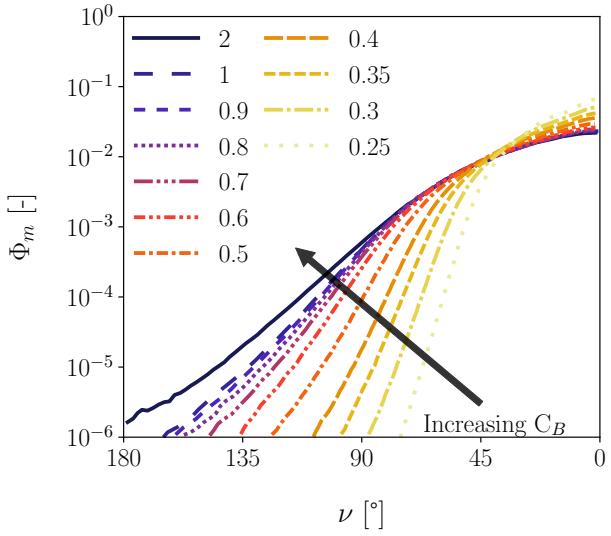

(a)

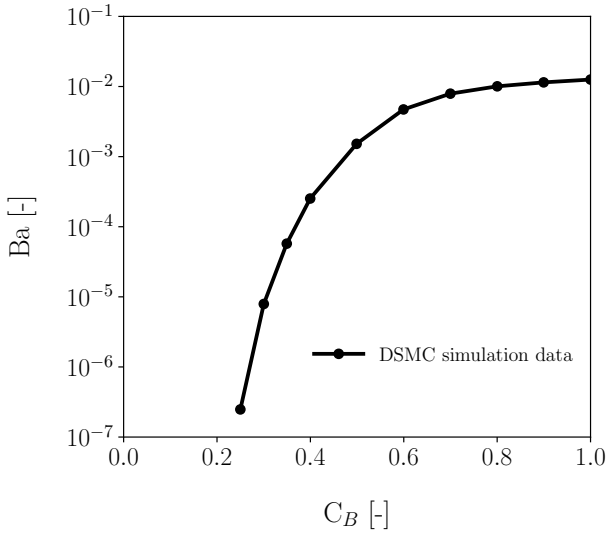

(b)

FIG. 10: Evolution of (a) angular mass flux and (b) backflow number Ba with plume adimensional number C_B.

particles will backflow, and setting the fraction of particle with a negative u that will indeed backflow as α leads to the following first model:

$$\mathrm{Ba}_{\text{model, 1}} \approx \frac{f}{\alpha} = \frac{\mathrm{erf}\left(\dfrac{-1}{\sqrt{2}\mathrm{C_B}}\right) + 1}{2\alpha} \tag{9}$$

The value of α can then be estimated by minimizing:

$$\sum_{p \in \text{Data points}} \left|\log_{10}\left(\mathrm{Ba}_{p,\ \text{DSMC}}\right) - \log_{10}\left(\mathrm{Ba}_{p,\ \text{model}}\right)\right| \tag{10}$$

Figure 11 represents, as Figure 10b, the backflow number Ba as a function of C_B for both the DSMC simulation

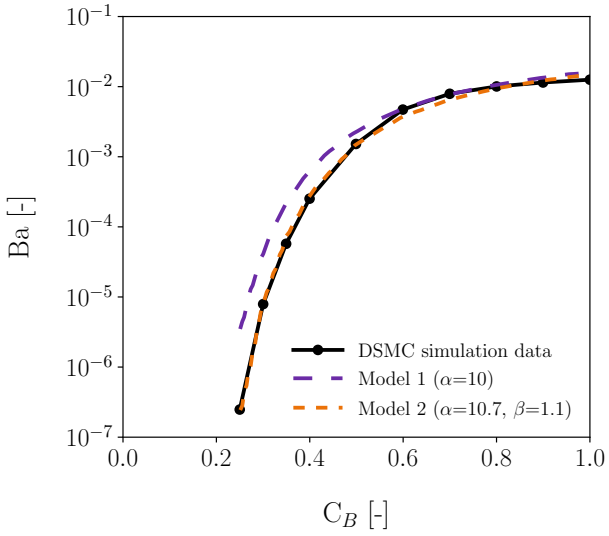

FIG. 11: Normalized backflowing mass flux vs. adimensional number C_B.

data and for the first model, with an estimated value of $\alpha = 10$. While the model predicts the correct amount of backflow for large values of C_B, it overestimates it when C_B becomes less than 0.6.

This could be explained by the fact that the fraction f of particles with negative u is directly dictated by C_B, and the PDF(u) is a Maxwellian distribution, therefore if f is small the only particles with negative u have only slightly negative velocities.

If f is larger, some particles will have more negative velocities. It is reasonable to assume that particles with highly negative u have a larger chance of backflowing, since they can collide one or several times before being pushed towards positive x. Therefore if C_B is small and particles only have slightly negative u, then less of said particles will indeed backflow. To account for this, an empirical correction factor $\beta \geq 1$ that artificially reduces f for small values of C_B can be added which leads to this second model:

$$\mathrm{Ba}_{\text{model, 2}} \approx \frac{\mathrm{erf}\left(\dfrac{-1}{\sqrt{2}\mathrm{C_B^{\beta}}}\right) + 1}{2\alpha} \tag{11}$$

Estimating the two coefficients by minimizing Equation (10) leads to $\alpha = 10.7$ and $\beta = 1.1$. With these input parameters, this second model is able to reproduce correctly the DSMC simulation data as shown in Figure 11.

D. Backflow sensitivity on plume composition

While the previous model is efficient for calculating backflow of single species plumes, computing C_B is not as

straightforward for species mix. A per-species approach can then be used. For each species, *e.g.* for a heavy and a light species, $C_{B,\text{ species}}$ is computed with:

$$C_{B,\text{ species}} = \frac{\sqrt{\frac{k_B T_{inj}}{m_{species}}}}{u_{inj}} \tag{12}$$

The model developed in Section IV C can then be applied to each species:

$$Ba_{species} \approx \frac{\text{erf}\left(\frac{-1}{\sqrt{2}C_{B,\text{ species}}^{\beta}}\right) + 1}{2\alpha} \tag{13}$$

The total backflow number can be computed by weighting the sum using the mass fraction of each species $Y_{species}$:

$$Ba = \sum_{species} Ba_{species} \cdot Y_{species} \tag{14}$$

Contrary to Section IV C where the injection properties were simplified to ease the derivation of the model, the input conditions are now the same as the reference case of Table I except when specified otherwise. The plume is thus composed of two species and the atmosphere is still not considered. The dimensionless number $C_{B,species}$ can be computed for each species, here $C_{B,h} = 0.21$ and $C_{B,l} = 0.76$. These two values are computed using the injection properties in segment 9 of Table I, since it has been shown that segment 9 provides most of the backflowing gas. Since $C_{B,h} < 0.4$, the heavy species backflow is negligible.

Several simulations with varying fraction of light species are performed. Between each case the mass flux is kept constant, therefore the injected particles density of the new mixture is as follows:

$$n = n_{ref} \cdot \frac{X_{l,\text{ ref}} \cdot m_l + (1 - X_{l,\text{ ref}}) \cdot m_h}{X_l \cdot m_l + (1 - X_l) \cdot m_h} \tag{15}$$

where X_l is the desired molar fraction of light species, $X_{l,\text{ ref}}$ the reference one (*i.e.* 0.34), m_l the molecular mass of the light species and m_h that of the heavy species. n_{ref} corresponds to the last column of Table I. These simulations are presented in Figure 12, where Figure 12a which represents the outwards mass flux for different plume compositions. The evolution of Ba with the fraction of light species in the mixture is shown in Figure 12b. The model described by Equations (13) and (14) is also depicted in this graph, with $\alpha = 3.5$, which means around one third of the particles with negative velocities do backflow, and still $\beta = 1.1$. These values of α and β have been found by minimizing Equation (10) and assuming α and β are the same for every species.

A possible explanation to why in this case the fitting value of α is three times lower than in the previous section is that in this case v, *i.e.* the velocity in the r direction, is non zero therefore particles with a negative u are more likely to backflow.

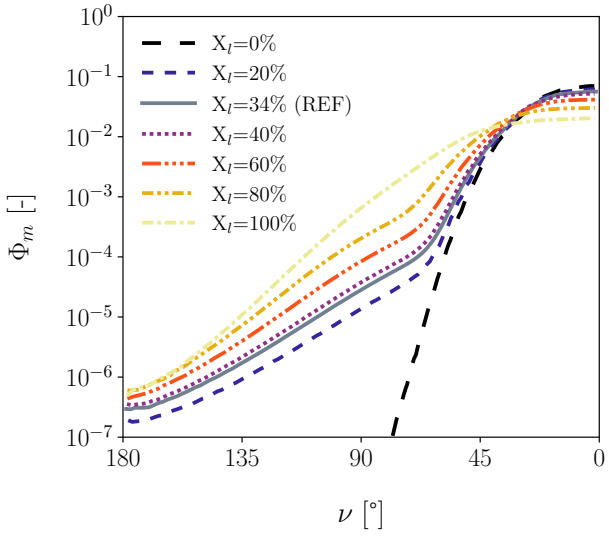

(a)

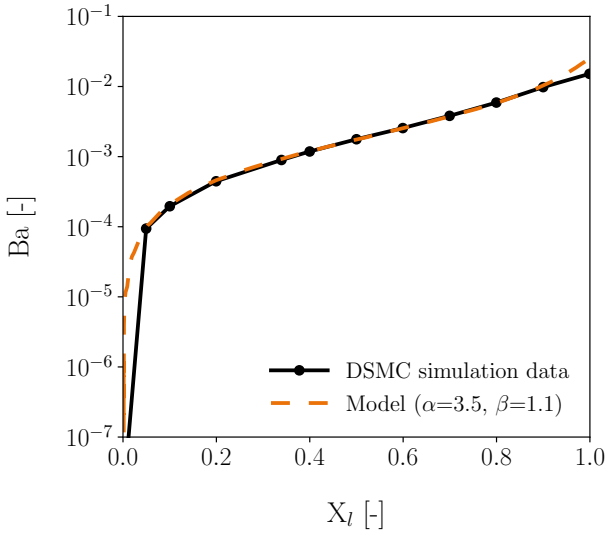

(b)

FIG. 12: (a) Evolution of angular mass flux with plume composition. The reference case $X_l = 34\,\%$ corresponds to the case in Section II B. (b) Backflow number Ba for several plume compositions, from simulations and using the model (eq. (14)) with $\alpha = 3.5$ and $\beta = 1.1$.

E. Backflow sensitivity on plume density

DSMC simulations of engine's plume can be costly or even unaffordable due to the high density of the core of the plume. Figure 13 shows the outwards normalized mass flux for several configurations with different input

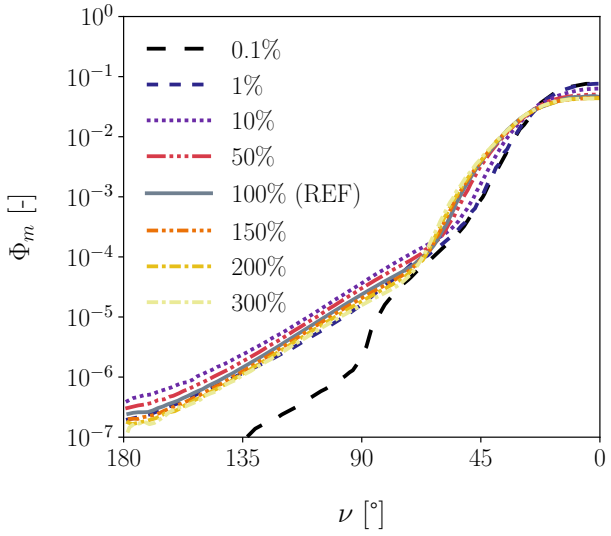

FIG. 13: Evolution of normalized outwards mass flux with plume density. The reference 100 % case corresponds to the case in Section II B.

TABLE IV: Correspondence between input density and local Knudsen number.

Relative density	$n_{\text{plume}}[\text{m}^{-3}]$	Kn_{plume}
0.1 %	2.333×10^{20}	8.1
1 %	2.333×10^{21}	8.1×10^{-1}
10 %	2.333×10^{22}	8.1×10^{-2}
50 %	1.166×10^{23}	1.6×10^{-2}
100 %	2.333×10^{23}	8.1×10^{-3}
150 %	3.499×10^{23}	5.4×10^{-3}
200 %	4.666×10^{23}	4.1×10^{-3}
300 %	6.999×10^{23}	2.7×10^{-3}

density of plume gas. The reference case of Table I corresponds to the 100 % case. The correspondence between plume density and local Knudsen number at NEP is listed in Table IV.

Plume density does not seem to modify in a significant manner the shape of the outwards mass flux of plume gases when the plume Knudsen number is smaller 1.6×10^{-2}. Consequently we can consider that Ba is constant as long as $\text{Kn}_{\text{plume}} \leq 10^{-2}$. This limit is of the order of the typical *continuous-transitional* threshold. This is expected since the derivation in Equation (5) considers the velocity distribution in the NEP to be a Maxwellian distribution, which is true only when the fluid is at the local thermal equilibrium.

This result supports that a reduced density DSMC simulation can be performed to predict backflow of a high density plume, without changing neither the backflow number Ba nor the shape of the angular mass flux curve, as long as the density in the NEP is sufficiently high for the fluid to be al local thermal equilibrium. This reduction in density allows for a large reduction in computational cost.

TABLE V: Atmospheric number density and Knudsen number corresponding to several altitudes[36].

Altitude [km]	n_{atmo} [m^{-3}]	Kn_{atmo}
-	0	∞
183	1.257×10^{16}	1×10^{3}
150	5.186×10^{16}	4×10^{2}
130	1.930×10^{17}	1×10^{2}
120	5.107×10^{17}	3×10^{1}
110	2.144×10^{18}	8
100	1.189×10^{19}	1

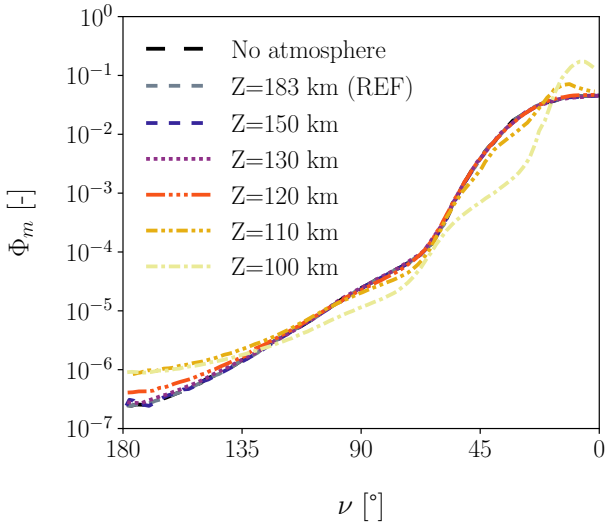

FIG. 14: Evolution of normalized outwards mass flux with different atmosphere densities. The reference 183 km case corresponds to the case in Section II B.

F. Backflow sensitivity on atmosphere density

The atmosphere influence on backflow is still to be considered. Several simulations at different altitudes are performed to assess this effect. In each case, all parameters of the simulations are exactly the same as those described in Section II B, except for the atmosphere density which is modified according to Table V. The atmospheric Knudsen number, $\text{Kn}_{\text{atmo}} = \lambda_{\text{atmo}}/R$, ranges over several orders of magnitude. A simulation without atmosphere is also carried out. Figure 14 represents the normalized outwards mass flux of plume species versus the view angle for all configurations described in Table V.

For all altitudes higher than 130 km, that is to say when $\text{Kn}_{\text{atmo}} \geq 100$, the normalized angular outwards mass flux is identical even at very large view angles ν. When the altitude decreases, starting at $\text{Kn}_{\text{atmo}} \approx 30$, this is no longer true. First the total backflowing mass

flux at view angles larger than 90°, *i.e.* Ba, is reduced. This means increasing the atmosphere density reduces backflow, which is an expected phenomenon since at low altitudes, *i.e.* in the continuum regime, backflow is not present. Nevertheless, this reduction in backflow is not identical at all view angles:

- The mass flux at $\nu < 30°$ is increased due to the interaction between the plume and the atmosphere, which pushes the plume particles towards positive x.
- At view angles $30° < \nu < 120°$ the mass flux is decreased for the same reason.
- At view angles $\nu > 120°$, the mass flux increases with the atmosphere density. This is explained by the fact that a collision between a plume particle and an atmospheric particle going almost straightly towards $+x$ tends not to modify u of the plume particle and tends to centre v of the plume particle to 0. Therefore if a plume particle has, before collision, a velocity with a slightly negative u and a positive v (thus heading towards $90° < \nu \lesssim 120°$), it would have after collision with a high impact parameter the same u but v almost to 0, thus heading towards $\nu \approx 180°$. Since the collision does not necessarily put v to precisely 0, the direction after collision can differ from 180° which explains why the normalized mass flux is increased starting at around $\nu > 120°$.

The effect of the collisions between the atmosphere particles and the plume particles on the velocity distribution of the plume particles is depicted in Figure 15, where the PDF is computed on the side of the vehicle. The lower the altitude, the more collisions occur, which tends to bring the two gases to equilibrium. In the vehicle's reference frame, the atmosphere has more kinetic energy, which explains why the velocity distribution widens at low altitude: the plume heats up. One can see in Figure 15 some particles with very large u, which, due to the position of the sampling region, cannot exist without collisions with the atmosphere. Nonetheless, the $\mathrm{Kn}_{\mathrm{atmo}}$ value at 100 km is 1, which is a large value that would suggest very few interaction between the atmosphere and the plume. This means that the freestream Knudsen number is not the only relevant parameter regarding atmosphere's influence on backflow. The PDF calculation zone of Figure 15 includes the frontal region which is filled with more particles due to compression effects, therefore the local atmospheric Knudsen number is reduced.

If the same figure is traced but for a region further from the vehicle, another phenomenology is seen as in Figure 16. In this case no plume particles have positive u. This means that in this region, the atmosphere and the plume species do not collide. The particles that are present here originate from the plume and went through the compression region, with some that collided with the

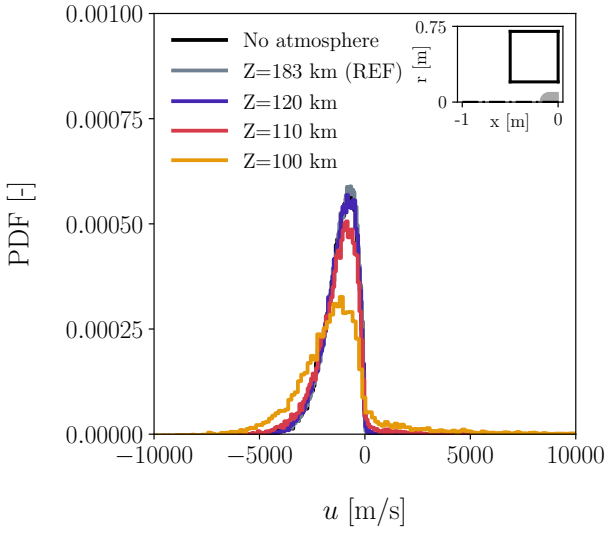

FIG. 15: PDF(u) of plume particles in the $(x, r) \in [-0.5, 0] \times [0.2, 0.7]$ region depicted in the subplot.

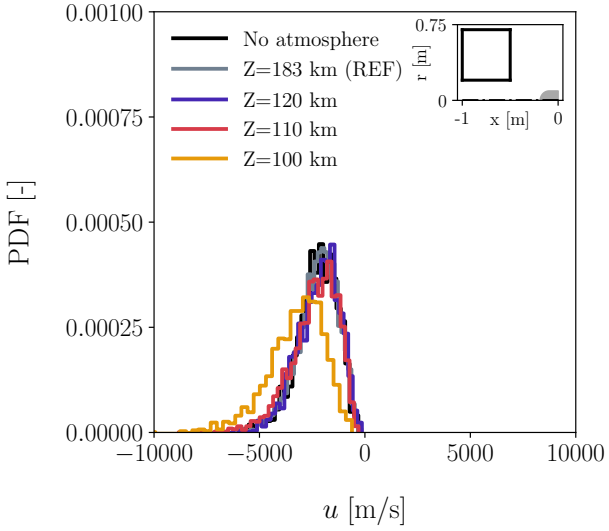

FIG. 16: PDF(u) of of plume particles in the $(x, r) \in [-1, -0.5] \times [0.2, 0.7]$ region depicted in the subplot.

atmosphere, which explains the shape of the PDF for negative u which is the same as in Figure 15.

Consequently the atmospheric density, *i.e.* the farfield atmospheric Knudsen number, is not the only relevant parameter for the atmosphere influence on backflow. The local atmospheric Knudsen number, particularly in the region of compression in front and on the sides of the vehicle, is also of interest. Two Knudsen numbers seem to determine the influence of atmosphere. The first one, which dictates whether or not the compression region pushes backflow towards low view angles ν, would be the

compression Knudsen number, *i.e.* $\mathrm{Kn_{comp}} = \mathrm{Kn_{atmo}}/c$ where c is computed as the ratio of the freestream density over the density at the nose of the vehicle. The second one is the freestream atmospheric Knudsen number $\mathrm{Kn_{atmo}}$. The atmosphere thus starts impacting backflow if the compression Knudsen number is less than 1.

G. Procedure for backflow prediction using the semi-analytical model

The overall methodology to predict the backflow behaviour based on the plume properties at NEP is summarized by the flowchart in Figure 17. First, if none of the species has a $\mathrm{C_B}$ value larger than 0.4, the plume can be considered not to backflow. Then for each species with a large value of $\mathrm{C_B}$ the backflow number Ba can be estimated using Equation (14). This model however relies on two parameters α and β, which can be estimated using a reduced density DSMC simulation with a maximum plume Knudsen number of 10^{-2}. This estimation is performed by minimizing this function:

$$\sum_{s\in\text{species}} Y_s \cdot \left|\log_{10}\left(\mathrm{Ba}_{s,\ \mathrm{DSMC}}\right) - \left(\mathrm{Ba}_{s,\ \mathrm{model}}(\alpha,\beta)\right)\right| \quad (16)$$

With the values of α and β, one can extrapolate the amount of backflow if the rocket engine properties, *i.e.* temperature, velocities and species mass fractions at NEP, are modified. Secondly, this model also allows for backflow estimation from minor species. For instance, some rocket engine can generate small quantities of atomic hydrogen, which can degrade payload surfaces[40], *e.g.* solar panels. Since it is a minor species, directly simulating H through the DSMC method is extremely costly. Fitting the model with only major species, then computing the $\mathrm{C_B}$ value of H using its input properties and using the model allows for evaluation of the amount of H going upstream.

Finally the atmosphere can modify backflow's shape and reduce it, *i.e.* it acts as a filter on backflow. The atmosphere seems to have an effect particularly in the higher density region located at the nose and on the sides close to the vehicle. The parameter that defines whether or not this influences backflow is the compression Knudsen number $\mathrm{Kn_{comp}}$. If the atmosphere is dense enough, *i.e.* if $\mathrm{Kn_{atmo}}$ is low, the farfield atmosphere also influences and reduces backflow.

V. APPLICATION OF THE MODEL TO THE JAXA CASE

For demonstration purposes, the model is applied to the full scale JAXA case introduced in Section I. To overcome the one-way hybrid CFD-DSMC assumption, a new simulation involving only DSMC with plume injection at NEP is conducted. Density is reduced by a factor of 100, such that $\mathrm{Kn_{plume}} \approx 10^{-3}$.

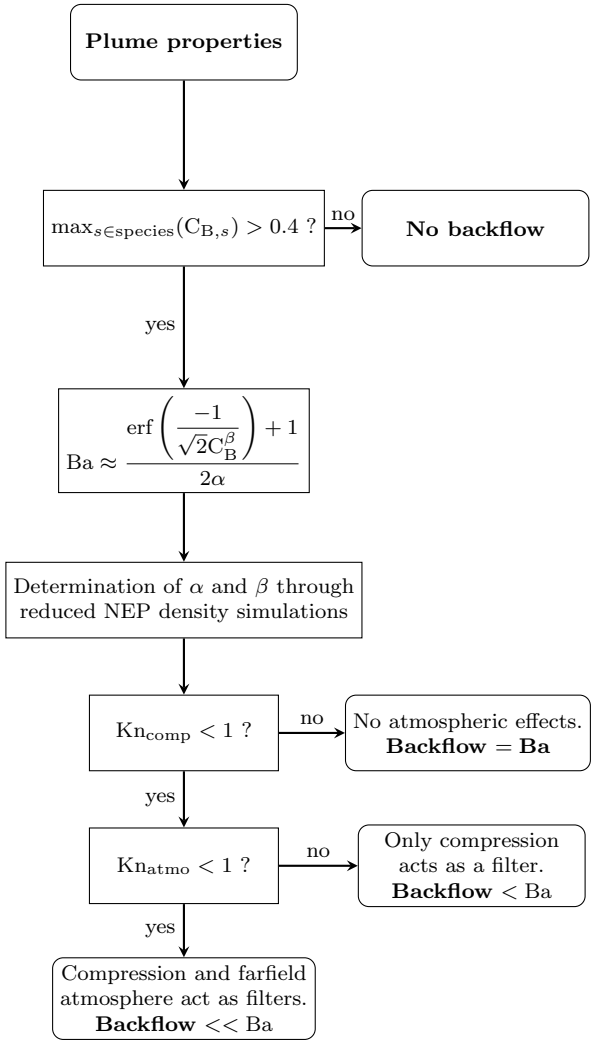

FIG. 17: Flowchart to determine the presence and mass of backflowing gas in atmospheric conditions.

TABLE VI: Computational data originating from reduced density simulation.

	H_2	H_2O	CO	N_2	HCl
Y	0.037	0.112	0.350	0.235	0.266
$\mathrm{C_B}$	1.44	0.48	0.38	0.38	0.34
Ba	1×10^{-2}	1×10^{-4}	8×10^{-6}	7×10^{-6}	2×10^{-6}

From the injection properties the mass fractions and $\mathrm{C_B}$ numbers of each species can be determined. From the simulation results the backflow number Ba for each species are found. These data are shown in Table VI.

Using this piece of information, the α and β coefficients of Equation (14) can be computed by minimizing Equation (16). In order to have data for validation, H_2O is not used in the species list to fit α and β. This gives

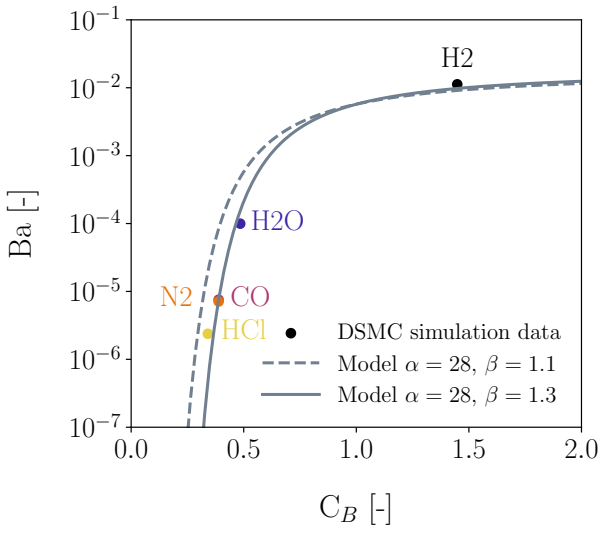

FIG. 18: Ba versus C_B issued from a reference DSMC simulation and the semi-analytical model, which is fitted using all species except H_2O.

$\alpha = 28$ and $\beta = 1.3$. Figure 18 represents in a single plot the DSMC simulation backflow data for each species, as well as the model using as before $\beta = 1.1$ and using the optimized value. Even though $\alpha = 28$ is larger than the values found in the previous sections, it makes sense because the vehicle geometry includes a nozzle lip with will prevent some particles with negative velocities to backflow. Other phenomena are also possibly at stake. While the $\beta = 1.1$ model provides good results for H_2, it tends to overestimate Ba by a factor of 3 to 10 for HCl, N_2, CO, and H_2O. On the other hand the model with the optimized value $\beta = 1.3$ provides a good estimation for Ba_{H2O}. This confirms that this model can be used to predict backflow for species not taken in the parameters fitting. For instance, the solid rocket motor which is used for this JAXA case produces some atomic hydrogen. From the input conditions, $C_{B,\,H} = 2.06$ which gives using the model $Ba_H = 0.127$. Knowing the total engine mass flux is $60\,\mathrm{kg\,s^{-1}}$ and $Y_H = 3 \times 10^{-4}$, the total mass flux of atomic hydrogen going upstream of the vehicle should be $2.3\,\mathrm{g\,s^{-1}}$.

Finally the atmospheric Knudsen number in the higher density region in this case is $Kn_{comp} = 20$, therefore neither the compression region nor the farfield atmosphere should have influence on backflow.

VI. CONCLUSION

This paper presents a DSMC simulation of a plume flow at high altitude on a large domain around a decimetre sized rocket with high temperature and high exit velocity two species plume. This simulation highlighted the presence of backflow, *i.e.* of plume gas going upstream. This backflow is composed exclusively of the lightest of the two species, and is in large majority from the near lip region of the nozzle-exit plane. A semi-analytical model to predict backflow through the dimensionless numbers Ba and C_B has been developed. It depends on two parameters α and β, which values can be determined *via* a reduced cost simulation at a lower plume density, since it has been found that Ba is density invariant in the limit of $Kn_{plume} \leq 10^{-2}$. Backflow sensitivity to atmosphere density has also been found to rely on two Knudsen numbers, one for the high density region close to the nose and sides of the vehicle and one for the freestream. Finally, the model has been tested on a meter sized high altitude solid rocket engine and succeeds in predicting the amount of backflow of H_2O. It also allows for estimation of backflow from minor species, which was unaffordable directly from DSMC simulations. These minor species can for instance be atomic hydrogen, which provides a large amount of backflow due to its low mass and can degrade payload surfaces. This model could however still be improved by investigating the precise effect of the geometry on α, and how the plume mixture influences β. High view angle backflow experimental measurements could also be used to validate the model.

AKNOWLEDGEMENTS

The authors would like to thank the French Defense Innovation Agency (AID), the French Procurement Agency for Armament (DGA) and the ONERA's scientific direction for funding and supporting the present work.

AUTHOR DECLARATIONS

Conflict of Interest

The authors have no conflicts to disclose.

Author Contributions

Antoine Clout: Conceptualization (equal), Formal analysis (equal), Methodology (equal), Software (lead), Visualization, Writing – original draft

Adrien Langenais: Conceptualization (equal), Formal analysis (equal), Methodology (equal), Software (supporting), Supervision (equal), Writing – review & editing (equal)

Yann Dauvois: Conceptualization (equal), Formal analysis (equal), Methodology (equal), Software (supporting), Supervision (equal), Writing – review & editing (equal)

Luc Mieussens: Conceptualization (equal), Formal analysis (equal), Methodology (equal), Supervision (equal), Writing – review & editing (equal)

Julien Labaune: Conceptualization (equal), Formal analysis (equal), Methodology (equal), Supervision (equal), Writing – review & editing (equal)

DATA AVAILABILITY STATEMENT

The data are within the article.

REFERENCES

[1] V. Rialland, A. Guy, D. Gueyffier, P. Perez, A. Roblin, and T. Smithson, "Infrared signature modelling of a rocket jet plume - comparison with flight measurements," Journal of Physics: Conference Series **676**, 012020 (2016).

[2] B. Fromentin-Denoziere, D. Gueyffier, and J. Simon, "Numerical modelling of the radar signature of rocket exhaust plumes," in *2012 International Conference on Electromagnetics in Advanced Applications* (IEEE, 2012).

[3] K. Kinefuchi, K. Okita, I. Funaki, and T. Abe, "Prediction of in-flight radio frequency attenuation by a rocket plume," Journal of Spacecraft and Rockets **52**, 340–349 (2015).

[4] K. Kinefuchi, I. Funaki, T. Shimada, and T. Abe, "Computational fluid dynamics and frequency-dependent finite-difference time-domain method coupling for the interaction between microwaves and plasma in rocket plumes," Physics of Plasmas **19**, 102112 (2012).

[5] D. Gueyffier, B. Fromentin-Denoziere, J. Simon, A. Merlen, and V. Giovangigli, "Numerical simulation of ionized rocket plumes," Journal of Thermophysics and Heat Transfer **28**, 218–225 (2014).

[6] A. Langenais, F. Vuillot, J. Troyes, and C. Bailly, "Accurate simulation of the noise generated by a hot supersonic jet including turbulence tripping and nonlinear acoustic propagation," Physics of Fluids **31**, 016105 (2019).

[7] R. Paoli, A. Poubeau, and D. Cariolle, "Large-Eddy Simulations of a Reactive Solid Rocket Motor Plume," AIAA Journal **58**, 1639–1656 (2020).

[8] J. E. Chirivella, "Molecular flux measurements in the back flow region of a nozzle plume," Technical report 33-620 (NASA, 1973).

[9] W. Guman and M. Begun, "Exhaust plume studies of a pulsed plasma thruster," in *13th International Electric Propulsion Conference* (AIAA (AIAA), 1978).

[10] L. Rudolph, L. Pless, and K. Harstad, "Pulsed Plasma Thruster Backflow Characteristics," Journal of Spacecraft and Rockets **17**, 447–452 (1980).

[11] A. B. Bailey, "Flow-angle measurements in a rarefied nozzle plume," AIAA Journal **25**, 1301–1304 (1987).

[12] S. Boraas, "Spacecraft contamination from scarfed nozzle exhausts," Journal of Spacecraft and Rockets **24**, 539–545 (1987).

[13] R. M. Jenkins, A. Ciucci, and J. E. Cochran, "Simplified model for calculation of backflow contamination from rocket exhausts in vacuum," Journal of Spacecraft and Rockets **31**, 265–270 (1994).

[14] G. A. Bird, *Molecular Gas Dynamics and the Direct Simulation of Flows* (Oxford University Press, 1994).

[15] J. E. Hueser, L. T. Melfi, G. A. Bird, and F. J. Brock, "Rocket nozzle lip flow by direct simulation Monte Carlo method," Journal of Spacecraft and Rockets **23**, 363–367 (1986).

[16] M. Ivanov, A. Kudryavtsev, G. Markelov, P. Vashchenkov, D. Khotyanovsky, and A. Schmidt, "Numerical Study of Backflow for Nozzle Plumes Expanding into Vacuum," in *37th AIAA Thermophysics Conference* (AIAA, 2004).

[17] P. V. Vashchenkov, "DSMC and Navier-Stokes Study of Backflow for Nozzle Plumes Expanding into Vacuum," in *AIP Conference Proceedings* (AIP, 2005).

[18] T. E. Schwartzentruber and I. D. Boyd, "A hybrid particle-continuum method applied to shock waves," Journal of Computational Physics **215**, 402–416 (2006).

[19] J. Papp, R. Wilmoth, C. Chartrand, and S. Dash, "Simulation of High-Altitude Plume Flow Fields Using a Hybrid Continuum CFD/DSMC Approach," in *42nd AIAA/ASME/SAE/ASEE Joint Propulsion Conference & Exhibit* (AIAA, 2006).

[20] J. Burt and I. D. Boyd, "A hybrid particle approach for continuum and rarefied flow simulation," Journal of Computational Physics **228**, 460–475 (2009).

[21] G. Abbate, C. R. Kleijn, and B. J. Thijsse, "Hybrid Continuum/Molecular Simulations of Transient Gas Flows with Rarefaction," AIAA Journal **47**, 1741–1749 (2009).

[22] S.-S. Xu, Z.-N. Wu, Q. Li, and Y.-J. Hong, "Hybrid continuum/DSMC computation of rocket mode lightcraft flow in near space with high temperature and rarefaction effect," Computers Fluids **38**, 1394–1404 (2009).

[23] F. La Torre, S. Kenjereš, J.-L. Moerel, and C. R. Kleijn, "Hybrid simulations of rarefied supersonic gas flows in micro-nozzles," Computers Fluids **49**, 312–322 (2011).

[24] V. Charton, A. Awad, and J. Labaune, "Optimisation of a hybrid NS–DSMC methodology for continuous–rarefied jet flows," Acta Astronautica **195**, 295–308 (2022).

[25] U. Rasthofer, P. Ohmer, and H. Siegmann, "A Hybrid Continuum-Kinetic Approach for High Altitude Rocket Exhaust Plume Simulation," in *Use of Computational Fluid Dynamics for Design and Analysis: Bridging the Gap Between Industry and Developers* (STO, 2022).

[26] I. Nompelis, M. D. Kroells, T. E. Schwartzentruber, and G. V. Candler, "Towards a Fully Consistent DSMC-CFD Hybrid Method for Hypersonic Nonequilibrium Reacting Flows," in *AIAA SCITECH 2023 Forum* (AIAA, 2023).

[27] A. Clout, A. Langenais, Y. Dauvois, L. Mieussens, and J. Labaune, "Hybrid NS-DSMC simulation of a full scale solid rocket motor reactive exhaust at high altitude," in *10th EUCASS* (EUCASS, 2023).

[28] K. Kinefuchi, H. Yamaguchi, M. Minami, K. Okita, and T. Abe, "In-flight S-band telemetry attenuation by ionized solid rocket motor plumes at high altitude," Acta Astronautica **165**, 373–381 (2019).

[29] M. Sabouri and M. Darbandi, "Numerical study of species separation in rarefied gas mixture flow through micronozzles using DSMC," Physics of Fluids **31** (2019), 10.1063/1.5083807.

[30] S. J. Plimpton, S. G. Moore, A. Borner, A. K. Stagg, T. P. Koehler, J. R. Torczynski, and M. A. Gallis, "Direct Simulation Monte Carlo on petaflop supercomputers and beyond," Physics of Fluids **31**, 086101 (2019).

[31] K. Koura and H. Matsumoto, "Variable soft sphere molecular model for inverse-power-law or Lennard-Jones potential," Physics of Fluids A: Fluid Dynamics **3**, 2459–2465 (1991).

[32] C. Borgnakke and P. S. Larsen, "Statistical collision model for Monte Carlo simulation of polyatomic gas mixture," Journal of computational Physics **18**, 405–420 (1975).

[33] J. G. Parker, "Rotational and Vibrational Relaxation in Diatomic Gases," The Physics of Fluids **2**, 449–462 (1959).

[34] R. C. Millikan and D. R. White, "Systematics of Vibrational Relaxation," The Journal of Chemical Physics **39**, 3209–3213 (1963).

[35] "Japan Aerospace Exploration Agency Special Document (ISSN 1349-113X – JAXA-SP-07-023)," Tech. Rep. (JAXA, 2008).

[36] "U.S. Standard Atmosphere," Tech. Rep. (NOAA, NASA, USAF, 1976).

[37] M. Châtelet, J. Kieffer, and B. Oksengorn, "Vibrational energy relaxation of highly compressed gaseous H_2 and N_2," Chemical Physics **79**, 413–429 (1983).

[38] I. B. Sebastião, L. Qiao, and A. Alexeenko, "Direct Simulation Monte Carlo modeling of H_2–O_2 deflagration waves," Combustion and Flame **198**, 40–53 (2018).

[39] J. A. Lordi and R. E. Mates, "Rotational Relaxation in Nonpolar Diatomic Gases," The Physics of Fluids **13**, 291–308 (1970).

[40] C. Chung, S. Kim, R. Stubbs, and K. de Witt, "Analysis of plume backflow around a nozzle lip in a nuclear rocket," in *29th Joint Propulsion Conference and Exhibit* (AIAA, 1993).